ACS OMEGA

http://pubs.acs.org/journal/acsodf

Article

Experiment Investigation of SiO_2 Containing Amino Groups as a Kinetic Promoter for CO_2 Hydrates

Lanyun Wang, Xiaoran Lu, and Yongliang Xu*

Cite This: *ACS Omega* 2021, 6, 19748−19756

Read Online

ACCESS | Metrics & More | Article Recommendations

ABSTRACT: To diminish the greenhouse effect by reducing CO_2 emission into the air based on a capture and sequestration method through hydrates, the thermodynamic and kinetic effects of additives on CO_2 hydrate formation under 1.5 MPa in the presence of 5, 6, 8, 10, and 20 wt % RNS-A (reactive SiO_2 containing amino groups) were studied, and the stirrer speed was set to 800 rpm. This paper calculated the gas consumption and explained the possible mechanisms of RNS-A on CO_2 hydrates. The results showed that RNS-A was a kinetic additive instead of a thermodynamic one. It was found that 5−10 wt % RNS-A all shortened the induction time of hydrates, but only 5 and 6 wt % RNS-A increased the gas consumption of CO_2 hydrates. Although we observed the shortest induction time at a 10 wt % RNS-A system, the lowest gas consumption indicated its weak CO_2 capture and storage ability. In addition, when the concentration was 6 wt %, RNS-A had the highest gas consumption and its reaction time was relatively short. Considering the induction time and gas consumption, 6 wt % RNS-A was the optimal RNS-A concentration for CO_2 capture and sequestration, which was the most suitable for practical applications.

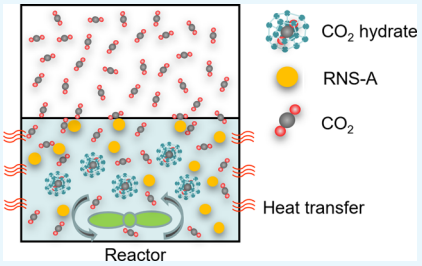

1. INTRODUCTION

Gas hydrates are a new method to capture and store CO_2. They are an environmentally friendly and highly reusable technology with a simple operation, relatively higher storage density, safer process, and lower cost. However, the slow hydrate formation rate and gas storage capacity are the current bottlenecks for industrial application in gas capture, separation, and storage.

Chemical additives are considered to be more attractive to change the thermodynamic or kinetic characteristics of hydrate formation. Thermodynamic additives can change the temperature and pressure conditions for hydrate formation.[1] Thermodynamic additives (*e.g.*, TBAB, THF, CP, and acetone) usually require a large amount of dosage, leading to a high cost.[2−5] Kinetic additives can affect the surface tension and gas solubility of hydrates and ultimately affect the induction time and gas consumption of hydrate formation.[6] Kinetic additives (*e.g.*, SDS and SDBS) are harmful to the environment and are difficult to degrade naturally.[7] In addition, the hydrates doped with surfactants will produce many foams during the separation process. Foams can cause blockages and equipment pollution, which have a negative effect on the practical application of gas hydrates.[8−11] Rahimi Mofrad *et al.*[12] studied the effects of additives on the formation rate and stability of NGH (natural gas hydrate) in the presence of SL (sulfonated lignin) and SDS. The study found that both additives promote hydrate formation, but compared to SL, the hydrate formed in the SDS solution was less stable. In addition, the hydrate was loose and foamy, which brought some difficulties to the storage, transportation, and degassing of NGH.

A large part of hydrates in nature exists on the seafloor. The hydrate formation in the sandstone and the main component of sandstone is SiO_2. SiO_2 is a substance that exists widely in nature, which is convenient and easy to obtain, so it is chosen as an additive. Due to their small particle size and large specific surface area, nanoparticles can increase the contact area of gas−liquid, enhance heat dissipation, and promote the kinetics of gas hydrate formation.[13] Nashed *et al.*[14] reviewed the current research status of the effects of nanoparticles on hydrate formation, including carbon nanomaterials, metallic nanoparticles, and metallic and nonmetallic oxide nanomaterials. They stated that nanoparticles were kinetic additives with a weak impact on the equilibrium conditions of hydrates, and the concentration had little effect on thermodynamic effects. They also pointed out that nanoparticles are favorable for promoting hydrate formation of hydrophobic gases such as CH_4 rather than soluble gases such as CO_2. Wang *et al.*[15] carried out experiments on CH_4 hydrate formation in the hydrophilic nano-SiO_2 system with the concentration range of 1−6 wt % under the initial experimental conditions of 278.15 K and 5 MPa. They stated that the hydrophilic nano-SiO_2 inhibited CH_4 hydrate formation. Increasing the concentration may

Received: May 9, 2021
Accepted: July 14, 2021
Published: July 23, 2021

enhance the inhibiting effect, while the inhibition may be weakened when the concentration was very high.

Nanoscale SiO_2 has been proven to promote hydrate formation in the previous literature, while microscale SiO_2 is mostly used as a porous medium to participate in hydrate formation. Ge *et al.*[16] studied the formation and dissociation of CH_4 hydrates in a fixed bed of silica sand at 277.15 K and 8 MPa. Two sizes of silica sand (180−250 μm and 300−900 μm) were used in this experiment. They found that small-sized silica sand (180−250 μm) was more conducive to CH_4 hydrate formation and dissociation. Its hydrate formation amount, gas consumption, and CH_4 recovery rate were greater than those of large-sized silica sand. Mekala *et al.*[17] studied the formation kinetics of CO_2 hydrates in pure water, seawater, and porous media at 276.15 K and 6 MPa. The silica sand used in this work included three particle sizes: 160, 460, and 920 μm. They found that the gas consumption and water conversion rate increased with the decrease in the silica sand particle size during the hydrate formation process. Kumar *et al.*[18] studied the formation of CO_2 hydrates in three porous media silica gels (pore sizes of 60−120 mesh, 100−200 mesh, and 230−400 mesh, respectively) at 274 K and 3.55 MPa. They found that a larger surface area can consume more CO_2 during the hydrate formation process and shorten the induction time.

Many scholars had studied the effects of nano-SiO_2 and hundreds of micrometer-sized SiO_2 on hydrates, but no one had studied the effects of smaller micrometer-sized particles as an addition on hydrate formation. Also, Ren and Lu[19] found that SiO_2 hydrophilic particles had better dispersibility in water than hydrophobic ones. Here, RNS-A (reactive SiO_2 with amino groups) and its concentration on the thermodynamic and kinetic hydrate process of CO_2 under 1.5 MPa will be investigated. Furthermore, the relationship between hydrate formation time and CO_2 consumption will also be studied by the grey correlation degree method. Also, the possible mechanisms of hydrophilicity and alkalinity of RNS-A on CO_2 hydrates would be explained. This basic thermodynamic and kinetic work will conduce to help develop the application of hydrates in the capture and storage of CO_2.

2. RESULTS AND DISCUSSION

2.1. Particle Size, Shape, and Element Analysis of RNS-A. The particle size of RNS-A was measured by the Laser Diffraction Particle Size Analyzer (see Figure 1). The average particle size of RNS-A is 5.89 μm. Among them, only about 3.5% of RNS-A has a particle size at the nanoscale.

The functional groups on the surface of RNS-A were characterized by FT-IR (Fourier transform infrared spectroscopy) (see Figure 2). The absorption peak of 1105 cm^{-1} is caused by the asymmetric stretching vibration of Si−O−Si. The peaks at 797 and 467 cm^{-1} correspond to the symmetric stretching and bending vibrations of Si−O, respectively. The peaks at 1637 and 1568 cm^{-1} correspond to bending vibrations of N−H. The absorption peak of 3415 cm^{-1} may correspond to the stretching vibration of N−H or O−H. It can be seen from the peak area that the content of amino groups is very small compared to SiO_2.

In addition, the micromorphology of RNS-A was observed by SEM (scanning tunneling microscopy), and the elements were analyzed by EDS (energy dispersive spectroscopy) (see Figure 3). It can be seen that the shape of RNS-A is spherical, and there is no agglomeration. Its elements include Si, O, C, and N. The small content of N is observed in RNS-A, which comes from the amino functional group.

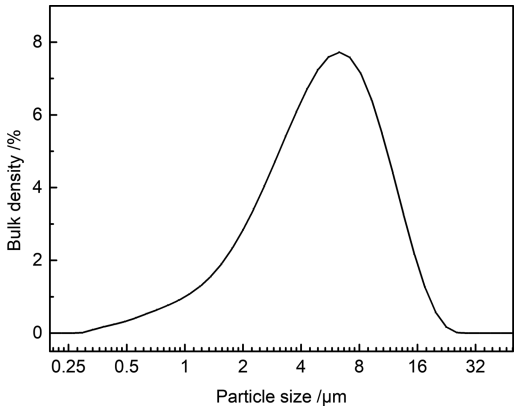

Figure 1. Particle size distribution of RNS-A.

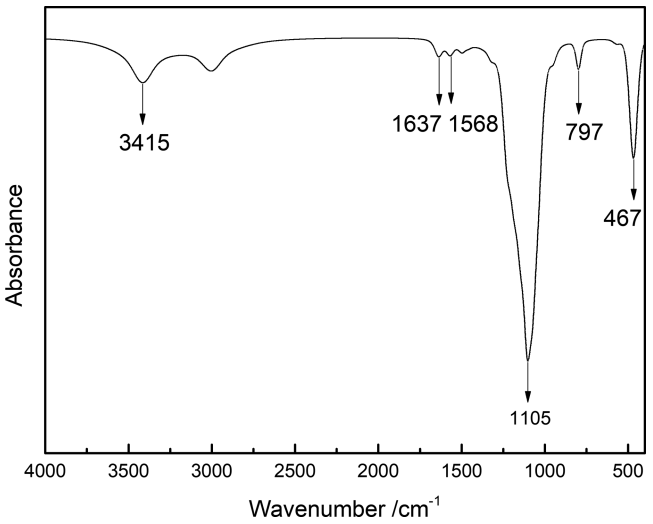

Figure 2. FT-IR images of RNS-A.

2.2. Reliability of the Experimental Equipment. To confirm the reliability of our experimental equipment, the phase equilibrium data of CO_2 in pure water were first tested and compared with the data from the reported literature (see Figure 4). It is seen that the phase equilibrium data are very close to the reported ones, proving that the experimental equipment used here is reliable.

2.3. Thermodynamic Analysis. Table 1 shows the phase equilibrium data of CO_2 hydrates in suspension in the presence of RNS-A with various concentrations. It is observed that all the equilibrium pressures and temperatures are very close to those of the pure water system. It indicates that the addition of RNS-A has little influence on the phase equilibrium condition of CO_2 hydrate formation, and the effect of RNS-A concentration is also very tiny. It can be inferred that RNS-A is not a thermodynamic additive for CO_2 hydrates.

2.4. Kinetic Analysis. Although RNS-A has a slight effect on hydrate equilibrium conditions, it can change the formation time and gas consumption during the hydrate process significantly. Figure 5 shows the formation time and gas consumption of CO_2 hydrates in all systems. Figure 5a shows the induction time, growth time, and total time. Figure 5b shows the gas consumption corresponding to each time.

https://doi.org/10.1021/acsomega.1c02440
ACS Omega 2021, 6, 19748−19756

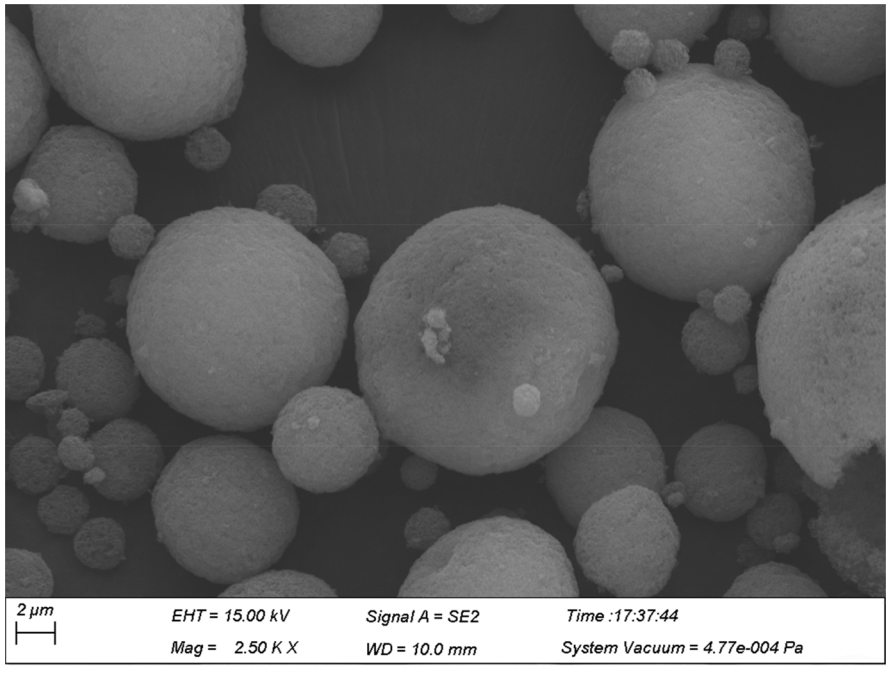

(a)

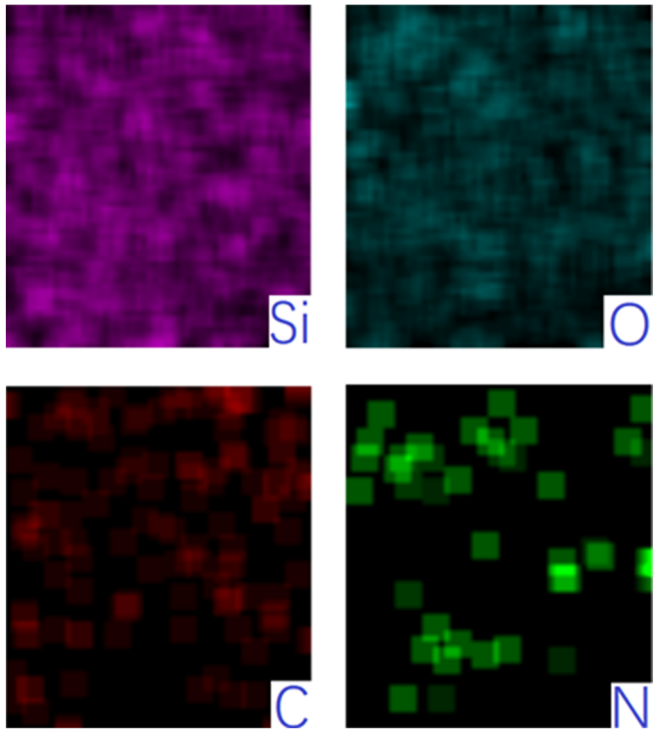

(b)

Figure 3. (a) SEM images of RNS-A; (b) EDS images of RNS-A (face analysis).

2.4.1. Induction Time. It is observed that the induction time of hydrate formation is 32,556 s in the pure water system. In the presence of RNS-A concentration of 5−10 wt %, the induction time is shorter than that of the pure water system, indicating that RNS-A has a significant promoting effect on the nucleation of CO_2 hydrates. In addition, the induction time decreases with RNS-A concentration increasing from 5 wt % to 10 wt %. There are very slight differences in the induction time for systems with 5, 6, and 8 wt % RNS-A, which are about 78% of the pure water system. When the RNS-A concentration is increased to 10 wt %, the induction time is reduced to 9198 s, which is much faster than that of the pure water system.

This is because the formation of CO_2 hydrates is an exothermic process that causes the temperature to rise, which reduces the driving force for hydrate formation. RNS-A has relatively good thermal conductivity and can remove heat more efficiently and faster.[14,21] Second, RNS-A with smaller particles can provide a larger gas−liquid contact surface area.[17] Third,

https://doi.org/10.1021/acsomega.1c02440
ACS Omega 2021, 6, 19748−19756

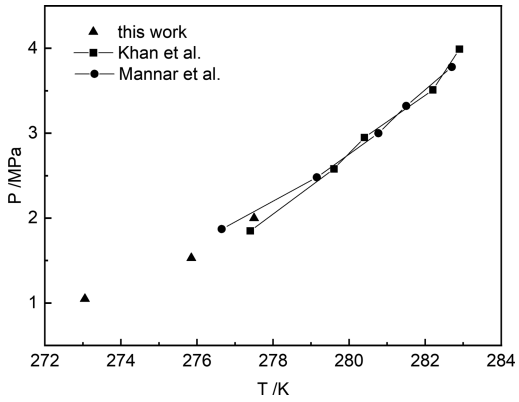

Figure 4. CO_2 phase equilibrium data in this work and other literature data: solid up-pointing triangle, this work; solid circle with a solid line, Mannar *et al.*; solid square with a solid line, Khan *et al.* Adapted from Mannar *et al.*[5] and Khan *et al.*[20]

Table 1. Phase Equilibrium Data of CO_2 Hydrates

system	*P*/MPa	*T*/K
pure water	1.53	275.75
5 wt % RNS-A	1.52	275.95
6 wt % RNS-A	1.50	275.40
8 wt % RNS-A	1.50	275.45
10 wt % RNS-A	1.51	275.55
20 wt % RNS-A	1.53	275.35

SiO_2 can also be the seeds of heterogeneous hydrate nucleation, providing nucleation sites, increasing the probability of nucleation, reducing the driving force required for the reaction, and shortening the induction time.[17,22−26] In addition, the Brownian motion of RNS-A and the stirring of the magnetic stirrer intensify the collision between RNS-A and destroy the bound water molecules on the surface.[27] Moreover, Bai *et al.*[28] found that the water film on the particles with weak hydrophilicity is less structured, has a weak restriction on water molecules bound on the surface, and thus promotes the gas−liquid interaction.

However, in the very concentrated suspension with 20 wt % RNS-A, the induction time of CO_2 hydrates increases to 49,728 s, which is vastly longer than that of the pure water system, indicating that the very high concentration is not favorable for CO_2 hydrating nucleation. It may be ascribed to the fact that although RNS-A with smaller particles can provide a larger gas−liquid contact surface area, the high concentration increases the difficulty of gas−liquid contact.[29] The concentration of 20 wt % may cause agglomeration of RNS-A, which can reduce the effective specific surface area and block the heat dissipation, thereby delaying the CO_2 hydrate nucleation.[30]

2.4.2. Gas Consumption. Gas consumption is another important index for selecting the optimal additives for hydrate formation. Large gas consumption implies an excellent ability for gas storage. Figure 5b shows the gas consumption corresponding to each time. We can find that except for the system of 20 wt %, Δn_g is less than Δn_h in other systems, indicating that a large number of hydrates are formed after nucleation. In the system with 20 wt % RNS-A, the growth of CO_2 hydrates is inhibited, with a very long induction time and thus relatively larger gas consumption during the inducting period. Figure 6 shows the change in gas consumption over time in each experimental system. Clearly, gas consumption

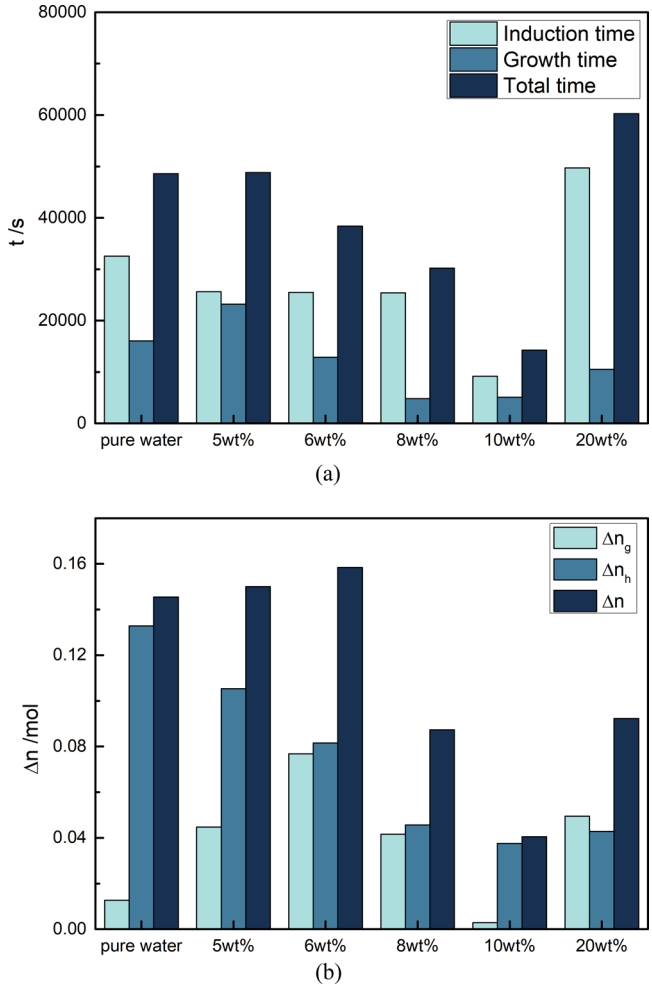

Figure 5. Relationship between formation time and gas consumption. (a) Induction time, growth time, and total time change with RNS-A concentration. (b) Gas consumption corresponding to each time (Δn_g is the gas consumption within the induction time; Δn_h is the gas consumption within hydrate growth time; Δn is the total gas consumption).

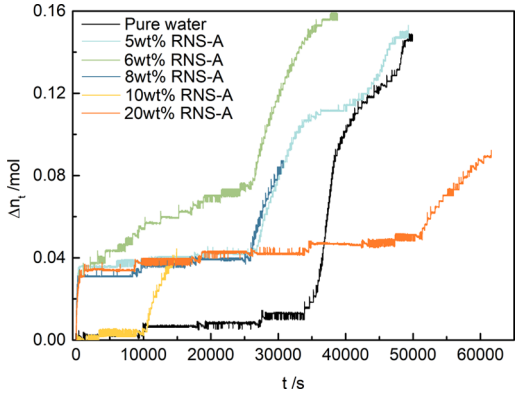

Figure 6. Change in gas consumption over time in different systems.

increases slowly at first and then sharply rises. The slow-growth phase causes gas dissolution and hydrate nucleation until the system reaches gas−liquid equilibrium, while the sharp-growth phase implies a large number of CO_2 hydrates being formed massively.

https://doi.org/10.1021/acsomega.1c02440
ACS Omega 2021, 6, 19748−19756

It is observed that within the range of 5−10 wt %, the overall trend is that CO_2 consumption decreases with increasing concentration of RNS-A. When the concentrations are 5 and 6 wt %, the gas consumption is slightly higher than that of the pure water system, wherein the gas consumption of 5 wt % RNS-A is slightly lower than that of 6 wt % RNS-A. It is because the lower concentration of amino groups has a relatively weaker effect on the inhibition of the activity of water molecules.[27] As the concentration of RNS-A increases, the water activity decreases with the increase in the number of amino groups. Furthermore, this is due to the Brownian motion of RNS-A, which reduces the membrane resistance at the gas−water interface and increases the gas consumption of CO_2 hydrates.[14,31,32] In addition, the growth time of hydrates with 5 and 6 wt % RNS-A is relatively longer than those of other systems, providing sufficient hydrating time for more CO_2 into the liquid phase to become hydrates. It is also worthy to note that the amino groups can adsorb CO_2 chemically and thus enhance CO_2 consumption.[33]

When the RNS-A concentration is increased to 8 wt %, CO_2 consumption is significantly reduced, reaching only 60% of the pure water system. When the concentration continues to increase to 10 wt %, CO_2 consumption is only half of 8 wt % RNS-A. Shorter growth periods are observed at 8 and 10 wt % compared to the pure water system, which possibly affects gas consumption. The gas−liquid interface is a suitable site for hydrate growth,[34] and the hydrate formed initially increases the resistance of CO_2 mass transfer from the gas phase into the liquid phase, which hinders the absorption of CO_2.[35] Therefore, the gas consumption of 8 and 10 wt % systems is significantly reduced.

When the RNS-A concentration is increased to 20 wt %, the gas consumption is 63% of the pure water system. The gas consumption at this time has a certain increase compared to 10 wt %, which is similar to the 8 wt % system. This is possible because of the fact that although the high-concentration RNS-A blocks CO_2 diffusion into the liquid phase, the increased hydrate formation time may provide an opportunity for more CO_2 to enter into the hydrate cages. Therefore, the gas consumption of the 20 wt % RNS-A system is higher than that of the 10 wt % RNS-A system.

The slope of Figure 6 represents the gas consumption rate during the hydrate formation process. It can be found that the hydrate is generated rapidly at first and then the rate becomes slower, which indicates that the formation of the initial hydrate hinders the mass transfer and slows down the rate of hydrate growth.

In summary, in the range of 5 to 10 wt %, RNS-A shortens the hydrate induction time. At 5 and 6 wt %, RNS-A increases the gas consumption of hydrates, wherein the gas consumption of 6 wt % RNS-A is slightly higher than that of 5 wt % RNS-A. In terms of induction time and gas consumption, 6 wt % RNS-A is the optimal concentration for CO_2 capture and storage. In addition, because RNS-A is also feasible economically, it can be taken into account to apply to industrial practice to capture, separate, and store CO_2.

2.5. Correlating Hydrating Time and Gas Consumption. Combining Figure 5a and Figure 5b, it is concluded that the hydrating time poses a direct impact on gas consumption, and usually, the rapid formation of hydrates will reduce the gas storage capacity of the hydrates. The critical task is to find a balance between hydrate formation time and gas consumption.

Based on the grey relational degree, the relationship between hydrate formation time and gas consumption was analyzed. The degree of relevance, r, ranges from 0 to 1, and is calculated and shown in Table 2. A larger r value indicates a higher correlation degree between time and gas consumption.

Table 2. Degree of Relevance, r, between Reaction Time and Gas Consumption

r	Δn_g/mol	Δn_h/mol	Δn/mol
induction time/s	0.6132	0.6276	0.7218
growth time/s	0.4635	0.7305	0.7715
total time/s	0.6308	0.6779	0.7882

It can be seen that the r between the total gas consumption and total time is the highest. Compared to the induction time we usually focus on, the r between growth time and gas consumption is more closely related. It is possible because gas consumption during the induction stage is much less, while a large amount of CO_2 would be consumed during the hydrate growth period. More gas consumption causes the growth period to affect the total gas consumption more than the induction period.

2.6. Mechanism of RNS-A on CO_2 Hydrates. In fact, the correlation between CO_2 hydrates and concentration is closely related to the property of RNS-A. As Qin *et al.*[33] reported, the amino group on the RNS-A surface, which is hydrophilic, has a certain inhibitory effect on the activity of water molecules. To a certain extent, this explains why 20 wt % RNS-A exhibits a strong inhibitory effect.

The possible specific inhibitory mechanism of RNS-A is shown in Figure 7. Figure 7a shows that RNS-A can bind the water molecules around RNS-A to form water films and reduce the activity of water molecules.[27] However, the hydrophilicity of amino groups is weaker, and the water film has less structured and weaker restrictions on water molecules bound on the surface, leading to a weaker inhibition effect on hydrate formation.[28] Figure 7b shows that the amino groups on the

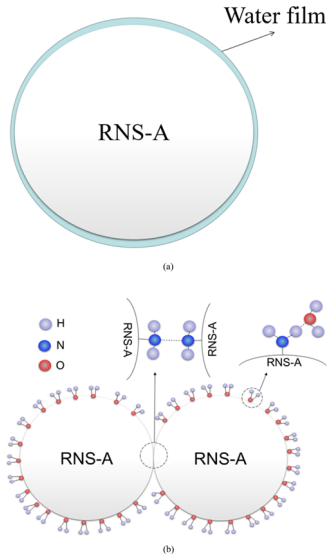

Figure 7. Possible inhibition mechanism of RNS-A on CO_2 hydrates. (a) Possible distribution of water films and CO_2 hydrates on the surface of RNS-A. (b) Surface characteristics of RNS-A: combination of amino groups with water molecules or adjacent amino groups.

https://doi.org/10.1021/acsomega.1c02440
ACS Omega 2021, 6, 19748−19756

surface of RNS-A form hydrogen bonds with water molecules against the influence of CO_2 molecules through weak Van der Waals force stably, competing with hydrates for host molecules. In addition, amino groups can form hydrogen bonds with adjacent amino groups. Hydrophilic groups can effectively destroy the structure of water, enhancing the inhibition effect of hydrates.[36]

Nevertheless, the formation of gas hydrates is an exothermic process that causes temperatures to rise, thus reducing the driving force for hydrate formation. RNS-A has relatively good thermal conductivity and larger contact surface area, which can remove heat more efficiently and faster.[14,17,21] In addition, RNS-A can act as seeds of heterogeneous hydrate nucleation, providing nucleation sites, increasing the probability of nucleation, and enhancing the driving force to promote hydrate formation.[23−26] Meanwhile, the Brownian motion of RNS-A can reduce the film resistance at the gas−liquid interface and enhance the mass transfer effect.[14,32] In addition, the Brownian motion of RNS-A and the stirring of the magnetic stirrer destroy the bound water molecules on the surface,[27] which promotes the hydrate formation.

Figure 8 shows the Brownian motion of RNS-A, and the stirring effect of the reactor aggravates the collision between RNS-A. Due to the less structured water film on the surface of RNS-A, the restriction on water molecules is weaker, and thus, the water film around RNS-A is easier to break.[28] In addition, due to the fact that amino groups can absorb CO_2 chemically, its surface can retain more CO_2 molecules, which results in concentrated CO_2 on the surface of RNS-A.[33] When the released water molecules are released and then form a cage, CO_2 molecules on the surface of RNS-A will enter the cage to create hydrates, which is a dynamic equilibrium process.

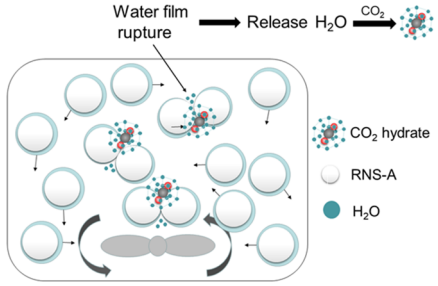

Figure 8. Possible promotion mechanism of RNS-A on CO_2 hydrates: the Brownian motion of RNS-A and water film rupture.

In cases of a low concentration of RNS-A, *i.e.*, 5 and 6 wt %, due to the fact that RNS-A has good thermal conductivity and large contact surface area, RNS-A can shorten the induction time and increase gas consumption, which acts as a kinetic promoter for CO_2 hydrates.

When the concentration continues to increase, *i.e.*, 8 and 10 wt %, the induction time continues to shorten. Due to the rapid formation of the initial hydrate, the diffusion of CO_2 from the gas phase to the liquid phase is hindered. Therefore, the gas consumption of the 8 and 10 wt % systems is reduced.

In the case of a very high concentration of RNS-A, *i.e.*, 20 wt % here, agglomeration of RNS-A will hinder the hydrate formation rate. In addition, too many RNS-A increases the resistance of Brownian motion[30] and limits CO_2 diffusion in solutions, consequently increasing the induction time and delaying hydrate growth. At this time, RNS-A acts as a kinetic inhibitor.

3. CONCLUSIONS

In this work, the effects of RNS-A on the phase equilibrium, induction time, and gas consumption of CO_2 hydrates were studied under 1.5 MPa. The experimental results showed that RNS-A had no significant effect on the phase equilibrium condition of CO_2 hydrates, whereas it could shorten the induction time, indicating that it was a kinetic promoter instead of a thermodynamic one. It was found that 5−10 wt % RNS-A all shortened the induction time of hydrates. Although 10 wt % RNS-A had the best effect on shortening the induction time, its gas consumption was inhibited, which was only 28.8% of that in the pure water system. In addition, only 5 and 6 wt % RNS-A increased the gas consumption of CO_2 hydrates. When the concentration increased to 20 wt %, RNS-A was transformed into the hydrate kinetic inhibitor completely, which shortened the induction time and reduced gas

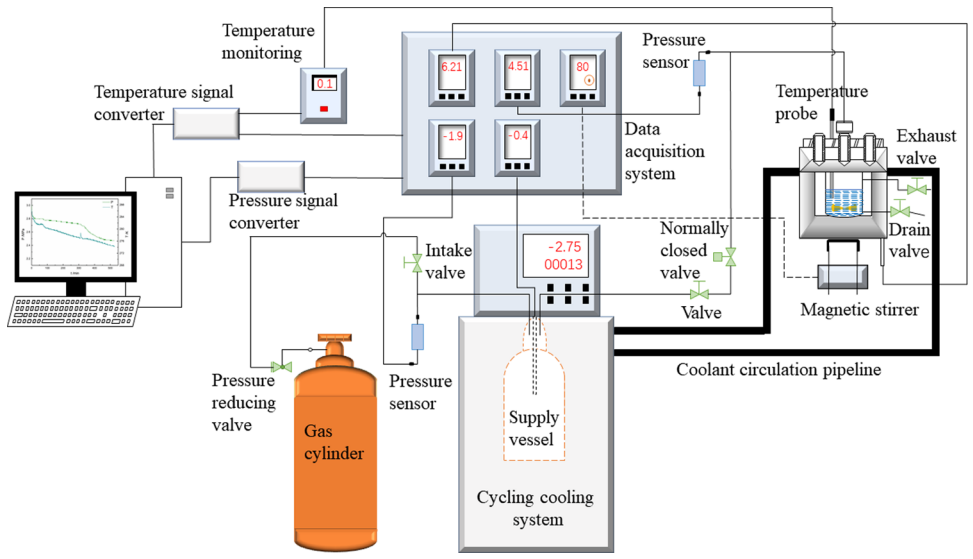

Figure 9. Schematic diagram of the hydrate kinetic experimental equipment.

https://doi.org/10.1021/acsomega.1c02440
ACS Omega 2021, 6, 19748−19756

consumption. A balance should be pursued between the induction time and gas storage capacity when considering appropriate promoters. Considering the induction time and gas consumption, 6 wt % RNS-A was the optimal RNS-A concentration for CO_2 capture and sequestration, which was the most suitable for practical applications.

In addition, RNS-A is only a kinetic promoter, and it can be taken into account to be compounded with a thermodynamic promoter to promote CO_2 hydrates in the future. This paper mainly studied the effect of amino groups on the formation of CO_2 hydrates, and we can also explore the effects of other functional groups on the formation of CO_2 hydrates and find better promoters for CO_2 capture and sequestration to be used in industrial practice as soon as possible.

4. EXPERIMENTAL SECTION

4.1. Experimental Materials. Deionized water, CO_2, and RNS-A were the main materials in this study. Deionized water was made in a laboratory. CO_2 (99.99%) was provided by Jining Xieli Special Gas Co., Ltd. RNS-A (reactive SiO_2 containing amino groups) was supplied by Henan Wangwu Nano Technology Co., Ltd.

4.2. Experimental Equipment. The schematic diagram of the hydrate kinetic experimental equipment is demonstrated in Figure 9. It consists of a high-pressure stirring reaction reactor, a cycling cooling system, and a data acquisition system. The high-pressure reactor is a cylindrical vessel with a volume of 100 mL, which can undertake pressures ranging from 0 to 20 MPa and temperatures from 253.15 to 423.15 K. The speed range of the stirring system (80YT25DV22) is 0−1500 rpm and its power is 25 W, which was supplied by JSCC Automation Co., Ltd. The cycling cooling system (CKDHX-1015 type) uses ethylene glycol as the coolant to maintain the low temperature. The temperature range of the cycling cooling system is 263.15−373.15 K, and the control precision is ±0.05 K. A Pt100 platinum resistance sensor was used to measure the temperature of the reactor and cycling cooling system with an accuracy of ±0.1 K. The pressure of this system was detected by a pressure sensor with an accuracy of ±5% (0−10 MPa). The temperature and pressure were monitored and recorded by a data acquisition system at an interval of 3 s.

4.3. Experimental Procedure. *4.3.1. Characterization of RNS-A.* The particle size of RNS-A was measured by the Laser Diffraction Particle Size Analyzer (Mastersizer 3000, Malvern Instruments Co., Ltd., England). The microscopic morphology of RNS-A was detected by SEM (Merlin Compact, Carl Zeiss NTS GmbH, Germany), and the component elements were analyzed with an attached facility OXFOFD EDS. The functional groups on the surface of RNS-A were characterized by FT-IR (Tensor 37, NETZSCH-Gerätebau GmbH, Germany).

4.3.2. Hydrate Formation Experiments. Before starting the experiment, 5, 6, 8, 10, and 20 wt % RNS-A suspensions were prepared, which needed to be ultrasonicated for 30 min. The experimental pipelines, valves, reactor sealing caps, and instrument interfaces were then checked to avoid gas leakage.

After that, the prepared suspension (50 mL) was introduced into the reactor, and the reactor was sealed immediately. To avoid the influence of air in the reactor, CO_2 was used to flush the reactor three times.

The temperature of the reactor was cooled by the cycling cooling system with a speed of 0.2 K/min. When the temperature of the cooling system reached 279.15 K, the temperature dropping rate was changed to be 0.5 K/h according to the report of Yan[37] to ensure the sufficient hydrate formation time and gas consumption. When the temperature of the reactor approached 285.15 K, CO_2 with a pressure of 1.5 MPa was introduced into the reactor, and the magnetic stirrer was turned on immediately. The stirring speed was set to 800 rpm according to Jiang and Yan.[38,39] The temperature and pressure were collected by a data acquisition system. A sudden and sharp drop of pressure in the gas storage tank indicates that a large quantity of CO_2 was consumed due to the formation of CO_2 hydrates. When the pressure of the gas storage tank remained unchanged for 30 min, indicating that the hydrate process was finished, the data acquisition system was turned off, the stirring was stopped, and the gas inlet valve was closed.

4.4. Determination of Hydrate Induction Time. Induction time refers to the time required from the first equilibrium of the system to a large number of visible crystals appearing in the system.[3] The induction time was determined based on the macroscopic dynamic hydrating measurements. As shown in Figure 10, CO_2 dissolves in the solution and then

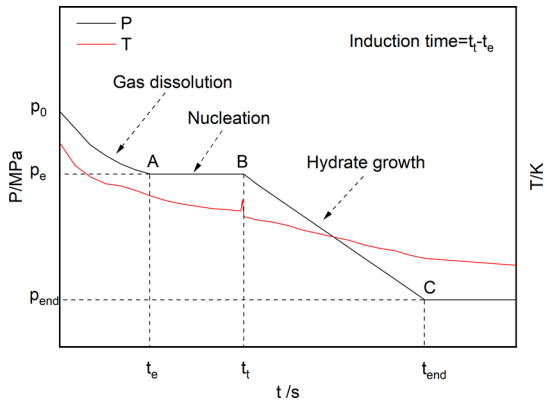

Figure 10. Determination of hydrate induction time.

reaches equilibrium at t_e.[40] After that, the pressure remains nearly unchanged between t_e and t_t until a large number of hydrates start to form at t_t when the pressure drops sharply. Here, the induction time is defined as the time gap between t_e and t_t.

4.5. Data-Processing Methods. *4.5.1. Kinetic Analyses.* Induction time, gas consumption, and gas consumption rate are the typical parameters obtained from hydrate formation kinetic measurements. According to the actual gas law, the amount of gas consumed in the hydrate formation process is calculated by eq 1,[41]

$$\Delta n_t = \frac{p_0 V}{Z_0 R T_0} - \frac{p_t V}{Z_t R T_t} \quad (1)$$

where Δn_t is the gas consumption from 0 to t (mol), V is the tank volume (mL), p_0 and p_t are pressures at the initial time and time t (MPa), T_0 and T_t are temperatures at the initial time and time t, respectively (K), Z_0 and Z_t are compression factors corresponding to T_0 and T_t, respectively, and R is the universal gas constant (8.3145 J/(mol·K)).

Among them, the compression factor can be calculated using the second virial coefficient, and the equations are shown in eqs 2 and 3,[42]

https://doi.org/10.1021/acsomega.1c02440
ACS Omega 2021, 6, 19748−19756

$$B = 5.7400 \times 10 - 3.8829 \times 10^4/T + 4.2899 \times 10^5/T^2 - 1.4661 \times 10^9/T^3 \quad (2)$$

$$Z = 1 + \frac{Bp}{RT} \quad (3)$$

where B is the second virial coefficient (cm^3/mol).

4.5.2. Grey Relational Analysis. To reveal the relationship between the reaction time and gas consumption, grey relational analysis was applied to analyze the degree of correlation between the two.

According to the grey system theory,[43−45] the parameters in the pure water system are taken as the reference sequence (X_0). The equation is shown in eq 4,

$$X_0(k) = \{X_0(1), X_0(2), X_0(3), ..., X_0(n)\} \quad (4)$$

The comparison sequence (X_i) is constituted by the parameters of each system with RNS-A. The equation is shown in eq 5,

$$X_i(k) = \{X_i(1), X_i(2), X_i(3), ..., X_i(n)\} \quad (5)$$

where k = 1, 2, 3, ..., n, and n is the number of the experimental group, here, n = 6, denoting six concentrations of pure water, 5, 6, 8, 10, and 20 wt %; i = 1, 2, 3, ..., m, and m is the number of comparison parameter, here, m = 3, denoting three kinds of times, induction time, growing time, and total time.

The original data are converted by a dimensionless method according to eq 6,

$$X_i'(k) = X_i(k)/X_0(k) \quad (6)$$

The absolute difference, $\Delta_i'(k)$, is calculated by the absolute gap between the comparison sequence X_i and the reference sequence X_0 at point k, as eq 7 shows.

$$\Delta_i'(k) = |X_0(k) - X_i(k)| \quad (7)$$

The correlation coefficient between the reference sequence X_0 and the comparison sequence X_i at point k is as shown in eq 8,

$$\varepsilon_i(k) = \frac{\min_i \min_k |X_0(k) - X_i(k)| + \rho \cdot \max_i \max_k |X_0(k) - X_i(k)|}{|X_0(k) - X_i(k)| + \rho \cdot \max_i \max_k |X_0(k) - X_i(k)|} \quad (8)$$

where ρ is the resolution coefficient (0.5).

Then, the degree of association, r, is calculated according to eq 9.

$$r_{0i} = \frac{1}{n} \sum_{k=1}^{n} \varepsilon_i(k) \quad (9)$$

AUTHOR INFORMATION

Corresponding Author

Yongliang Xu − *School of Safety Science and Engineering, Henan Polytechnic University, Jiaozuo 454003, China; Collaborative Innovation Center for Coal Safety Production & High-Efficient-Clean Utilization for Coal by Provincial and Ministerial Co-construction, Jiaozuo 454003, China; State Key Laboratory Cultivation Base for Gas Geology and Gas Control in Henan Polytechnic University, Jiaozuo 454003, China;* orcid.org/0000-0001-5484-4952; Phone: +0086 15993737530; Email: xylcumt@hpu.edu.cn

Authors

Lanyun Wang − *School of Safety Science and Engineering, Henan Polytechnic University, Jiaozuo 454003, China; Collaborative Innovation Center for Coal Safety Production & High-Efficient-Clean Utilization for Coal by Provincial and Ministerial Co-construction, Jiaozuo 454003, China; State Key Laboratory Cultivation Base for Gas Geology and Gas Control in Henan Polytechnic University, Jiaozuo 454003, China;* orcid.org/0000-0001-7862-5703

Xiaoran Lu − *School of Safety Science and Engineering, Henan Polytechnic University, Jiaozuo 454003, China;* orcid.org/0000-0002-2790-4558

Complete contact information is available at: https://pubs.acs.org/10.1021/acsomega.1c02440

Notes

The authors declare no competing financial interest.

ACKNOWLEDGMENTS

The authors wish to acknowledge gratefully the financial support of the research funding provided by the National Natural Science Foundation of China (nos. 52074108 and 51874124), the Doctoral Fund of Ministry of Education of China (nos. 2017M612397 and 2018T110725), and the funding from the Education Department of Henan Province (nos. 18A440005 and 19A440009). This work is also supported by the Research Funds of Henan Polytechnic University (J2019-5). The authors also appreciate all the reviewers and editors for their professional and constructive comments.

REFERENCES

(1) Sa, J.-H.; Hu, Y.; Sum, A. K. Assessing Thermodynamic Consistency of Gas Hydrates Phase Equilibrium Data for Inhibited Systems. *Fluid Phase Equilib.* **2018**, *473*, 294−299.

(2) Bavoh, C. B.; Partoon, B.; Lal, B.; Keong, L. K. Methane Hydrate-Liquid-Vapour-Equilibrium Phase Condition Measurements in the Presence of Natural Amino Acids. *J. Nat. Gas Sci. Eng.* **2017**, *37*, 425−434.

(3) Kamal, M. S.; Hussein, I. A.; Sultan, A. S.; von Solms, N. Application of Various Water Soluble Polymers in Gas Hydrate Inhibition. *Renewable Sustainable Energy Rev.* **2016**, *60*, 206−225.

(4) Lee, D.; Go, W.; Oh, J.; Lee, J.; Seo, Y. Thermodynamic Inhibition Effects of an Ionic Liquid (Choline Chloride), a Naturally Derived Substance (Urea), and Their Mixture (Deep Eutectic Solvent) on CH_4 Hydrates. *Chem. Eng. J.* **2020**, *399*, 125830.

(5) Mannar, N.; Bavoh, C. B.; Baharudin, A. H.; Lal, B.; Mellon, N. B. Thermophysical Properties of Aqueous Lysine and Its Inhibition Influence on Methane and Carbon Dioxide Hydrate Phase Boundary Condition. *Fluid Phase Equilib.* **2017**, *454*, 57−63.

(6) Sun, Q.; Chen, B.; Li, X.; Guo, X.; Yang, L. The Investigation of Phase Equilibria and Kinetics of CH_4 Hydrate in the Presence of Bio-Additives. *Fluid Phase Equilib.* **2017**, *452*, 143−147.

(7) Chaturvedi, E.; Prasad, N.; Mandal, A. Enhanced Formation of Methane Hydrate Using a Novel Synthesized Anionic Surfactant for Application in Storage and Transportation of Natural Gas. *J. Nat. Gas Sci. Eng.* **2018**, *56*, 246−257.

(8) Pandey, J. S.; Daas, Y. J.; von Solms, N. Screening of Amino Acids and Surfactant as Hydrate Promoter for CO_2 Capture from Flue Gas. *Processes* **2020**, *8*, 124.

(9) Cao, Q.; Xu, D.; Xu, H.; Luo, S.; Guo, R. Efficient Promotion of Methane Hydrate Formation and Elimination of Foam Generation Using Fluorinated Surfactants. *Front. Energy* **2020**, *14*, 443−451.
(10) Bhattacharjee, G.; Barmecha, V.; Kushwaha, O. S.; Kumar, R. Kinetic Promotion of Methane Hydrate Formation by Combining Anionic and Silicone Surfactants: Scalability Promise of Methane Storage Due to Prevention of Foam Formation. *J. Chem. Thermodyn.* **2018**, *117*, 248−255.
(11) Pandey, G.; Bhattacharjee, G.; Veluswamy, H. P.; Kumar, R.; Sangwai, J. S.; Linga, P. Alleviation of Foam Formation in a Surfactant Driven Gas Hydrate System: Insights via a Detailed Morphological Study. *ACS Appl. Energy Mater.* **2018**, *1*, 6899−6911.
(12) Rahimi Mofrad, H.; Ganji, H.; Nazari, K.; Kameli, M.; Rezaie Rod, A.; Kakavand, M. Rapid Formation of Dry Natural Gas Hydrate with High Capacity and Low Decomposition Rate Using a New Effective Promoter. *J. Pet. Sci. Eng.* **2016**, *147*, 756−759.
(13) Said, S.; Govindaraj, V.; Herri, J.-M.; Ouabbas, Y.; Khodja, M.; Belloum, M.; Sangwai, J. S.; Nagarajan, R. A Study on the Influence of Nanofluids on Gas Hydrate Formation Kinetics and Their Potential: Application to the CO_2 Capture Process. *J. Nat. Gas Sci. Eng.* **2016**, *32*, 95−108.
(14) Nashed, O.; Partoon, B.; Lal, B.; Sabil, K. M.; Shariff, A. M. Review the Impact of Nanoparticles on the Thermodynamics and Kinetics of Gas Hydrate Formation. *J. Nat. Gas Sci. Eng.* **2018**, *55*, 452−465.
(15) Wang, R.; Liu, T.; Ning, F.; Ou, W.; Zhang, L.; Wang, Z.; Peng, L.; Sun, J.; Liu, Z.; Li, T.; Sun, H.; Jiang, G. Effect of Hydrophilic Silica Nanoparticles on Hydrate Formation: Insight from the Experimental Study. *J. Energy Chem.* **2019**, *30*, 90−100.
(16) Ge, B.-B.; Zhong, D.-L.; Lu, Y.-Y. Influence of Water Saturation and Particle Size on Methane Hydrate Formation and Dissociation in a Fixed Bed of Silica Sand. *Energy Procedia* **2019**, *158*, 5402−5407.
(17) Mekala, P.; Busch, M.; Mech, D.; Patel, R. S.; Sangwai, J. S. Effect of Silica Sand Size on the Formation Kinetics of CO_2 Hydrate in Porous Media in the Presence of Pure Water and Seawater Relevant for CO_2 Sequestration. *J. Pet. Sci. Eng.* **2014**, *122*, 1−9.
(18) Kumar, A.; Sakpal, T.; Linga, P.; Kumar, R. Influence of Contact Medium and Surfactants on Carbon Dioxide Clathrate Hydrate Kinetics. *Fuel* **2013**, *105*, 664−671.
(19) Ren, J.; Lu, S. Dispersion Behaviors of Hydrophilic and Hydrophobic Particles in Water. *China Powder Sci. Technol.* **1999**, *5*, 6−9.
(20) Khan, M. S.; Bavoh, C. B.; Partoon, B.; Lal, B.; Bustam, M. A.; Shariff, A. M. Thermodynamic Effect of Ammonium Based Ionic Liquids on CO_2 Hydrates Phase Boundary. *J. Mol. Liq.* **2017**, *238*, 533−539.
(21) Kedzierski, M. A.; Brignoli, R.; Quine, K. T.; Brown, J. S. Viscosity, Density, and Thermal Conductivity of Aluminum Oxide and Zinc Oxide Nanolubricants. *Int. J. Refrig.* **2017**, *74*, 3−11.
(22) Yin, S.; Jin, Y.; Xia, B.; Ma, G.; Pan, Z. Study on the Formation Characteristics of Methane Hydrate in Different Porous Media in Artificial Seawater. *Chem. Eng. Oil Gas* **2020**, *49*, 38−43.
(23) Aliabadi, M.; Rasoolzadeh, A.; Esmaeilzadeh, F.; Alamdari, A. Experimental Study of Using CuO Nanoparticles as a Methane Hydrate Promoter. *J. Nat. Gas Sci. Eng.* **2015**, *27*, 1518−1522.
(24) Min, J.; Kang, D. W.; Lee, W.; Lee, J. W. Molecular Dynamics Simulations of Hydrophobic Nanoparticle Effects on Gas Hydrate Formation. *J. Phys. Chem. C* **2020**, *124*, 4162−4171.
(25) Park, S.-S.; An, E.-J.; Lee, S.-B.; Chun, W.; Kim, N.-J. Characteristics of Methane Hydrate Formation in Carbon Nanofluids. *J. Ind. Eng. Chem. (Amsterdam, Neth.)* **2012**, *18*, 443−448.
(26) Rahmati-Abkenar, M.; Manteghian, M.; Pahlavanzadeh, H. Nucleation of Ethane Hydrate in Water Containing Silver Nanoparticles. *Mater. Des.* **2017**, *126*, 190−196.
(27) Sun, H.; Wang, R.; Xu, X.; Wang, J.; Jiang, G.; Zhang, L.; Liu, T.; Ning, F. Effect of Hydrophilic Nano-SiO2 on CH4 Hydrate Formation. *J. China Univ. Pet., Ed. Nat. Sci.* **2018**, *42*, 81−87.
(28) Bai, D.; Chen, G.; Zhang, X.; Sum, A. K.; Wang, W. How Properties of Solid Surfaces Modulate the Nucleation of Gas Hydrate. *Sci. Rep.* **2015**, *5*, 12747.
(29) Farhang, F.; Nguyen, A. V.; Sewell, K. B. Fundamental Investigation of the Effects of Hydrophobic Fumed Silica on the Formation of Carbon Dioxide Gas Hydrates. *Energy Fuels* **2014**, *28*, 7025−7037.
(30) Pasieka, J.; Coulombe, S.; Servio, P. Investigating the Effects of Hydrophobic and Hydrophilic Multi-Wall Carbon Nanotubes on Methane Hydrate Growth Kinetics. *Chem. Eng. Sci.* **2013**, *104*, 998−1002.
(31) Javidani, A. M.; Abedi-Farizhendi, S.; Mohammadi, A.; Hassan, H.; Mohammadi, A. H.; Manteghian, M. The Effects of Graphene Oxide Nanosheets and Al_2O_3 Nanoparticles on the Kinetics of Methane + THF Hydrate Formation at Moderate Conditions. *J. Mol. Liq.* **2020**, *316*, 113872.
(32) Najibi, H.; Mirzaee Shayegan, M.; Heidary, H. Experimental Investigation of Methane Hydrate Formation in the Presence of Copper Oxide Nanoparticles and SDS. *J. Nat. Gas Sci. Eng.* **2015**, *23*, 315−323.
(33) Qin, H.; Zhang, X.; Zhang, P.; Wu, W. Progress in Amino Functionalized Solid Materials for CO_2 Capture. *Sci. Rep.* **2013**, *27*, 39−42.
(34) Bagherzadeh, S. A.; Englezos, P.; Alavi, S.; Ripmeester, J. A. Influence of Hydrated Silica Surfaces on Interfacial Water in the Presence of Clathrate Hydrate Forming Gases. *J. Phys. Chem. C* **2012**, *116*, 24907−24915.
(35) Veluswamy, H. P.; Lee, P. Y.; Premasinghe, K.; Linga, P. Effect of Biofriendly Amino Acids on the Kinetics of Methane Hydrate Formation and Dissociation. *Ind. Eng. Chem. Res.* **2017**, *56*, 6145−6154.
(36) Sa, J.-H.; Kwak, G.-H.; Han, K.; Ahn, D.; Lee, K.-H. Gas Hydrate Inhibition by Perturbation of Liquid Water Structure. *Sci. Rep.* **2015**, *5*, 11526.
(37) Yan, Z. *Fundamental Research on Absorption-hydration Method to Separate and Recover CO2 from IGCC Syngas*; China University of Petroleum: Beijing, Beijing, 2017: pp. 17.
(38) Jiang, L. L. *Experimental Research on Enhancing CO2 Hydrate Formation in Self-Priming Stirred Reactor*; Southwest Petroleum University: Chengdu, Sichuan, 2017: pp. 33.
(39) Yan, H. *Study on Methane Hydration Promoted by Slurry of N-Tetradecane*; Tianjin University: Tianjin, 2015: pp. 26.
(40) Pan, Y.; Liu, D.; Huang, W.; Xu, X.; Zhou, W. Dischmination of the Definition of Induction Time in Gas Hydrate Formation. *J. Univ. Shanghai Sci. Technol.* **2006**, *28*, 1−4,22.
(41) Babaee, S.; Hashemi, H.; Mohammadi, A. H.; Naidoo, P.; Ramjugernath, D. Kinetic and Thermodynamic Behaviour of CF_4 Clathrate Hydrates. *J. Chem. Thermodyn.* **2015**, *81*, 52−59.
(42) Dymond, J. H.; Wilhoit, R. C.; Marsh, K. N.; Wong, K. C. *Virial Coefficients of Pure Gases*; 1st ed.; Frenkel, M., Marsh, K. N., Eds.; NIST; 2002; Vol. *21A*: pp. 28.
(43) Wang, Y.; Liu, S.; Wang, C.; Li, J.; Pei, Y.; Song, X. Evaluation on Comprehensive Performance of 12 Silage Maize Varieties by Grey Relational Degree Analysis. *Shandong Agric. Sci.* **2020**, *52*, 78−82.
(44) Li, Y.; Jiao, S.; Geng, B. A Comparative Study of Four Multi-Scale Entropies Combined with Grey Relational Degree in Classification of Ship-Radiated Noise. *Appl. Acoust.* **2021**, *176*, 107865.
(45) Wu, L. F.; Liu, S. F.; Yao, L. G.; Yan, S. L. Grey Convex Relational Degree and Its Application to Evaluate Regional Economic Sustainability. *Sci. Iran.* **2012**, *20*, 44−49.

https://doi.org/10.1021/acsomega.1c02440
ACS Omega 2021, 6, 19748−19756